Inhibition of mixing in chaotic quantum dynamics

B. S. Helmkamp and D. A. Browne
Department of Physics and Astronomy, Louisiana State University, Baton Rouge, Louisiana 70803-4001
(Received 29 June 1994)

We study the quantum chaotic dynamics of an initially well-localized wave packet in a cosine potential perturbed by an external time-dependent force. For our choice of initial condition and with $\hbar$ small but finite, we find that the wave packet behaves classically (meaning that the quantum behavior is indistinguishable from that of the analogous classical system) as long as the motion is confined to the interior of the remnant separatrix of the cosine potential. Once the classical motion becomes unbounded, however, we find that quantum interference effects dominate. This interference leads to a long-lived accumulation of quantum amplitude on top of the cosine barrier. This pinning of the amplitude on the barrier is a dynamic mechanism for the quantum inhibition of classical mixing.

PACS number(s): 05.45.+b, 03.65.Sq

I. INTRODUCTION

While the inhibition of classical mixing in quantum chaotic dynamics is a generally accepted consequence of the linearity of the Schrödinger equation, how this inhibition is manifested in the dynamics of physical systems is not fully understood. This is a difficult question to address from a theoretical point of view because the complex nature of chaotic systems all but precludes an analytical approach, making general physical insights difficult to come by. However, by studying the semiclassical limit for simple low-dimensional systems, one can relate the quantum dynamics for specific case studies to generic features of the classical chaos and thereby discern generic semiclassical mechanisms that lead to the quantum inhibition of mixing.

The mechanism responsible for classical mixing is the repeated folding and stretching of the classical Lagrangian manifold in the vicinity of hyperbolic fixed points [1], and when the motion is chaotic, these folded structures, or "tendrils," eventually fill almost all the available phase space. The folding and stretching process leads to an abundance of caustics, or turning points, in the Lagrangian manifold. Since quantum effects are, loosely speaking, amplified at caustics, this can have a dramatic effect on the semiclassical description of the motion. One example of this is seen in the scattering of a wave packet off of a barrier [2]. When the wave packet reaches the turning point, it acquires a temporary standing wave modulation arising from the interference between the piece of the packet that has already reflected off the caustic and the piece that has not yet reached it. Thus the caustic temporarily amplifies the underlying quantum nature of an apparently classical object. Schulman quantified this propensity for nonclassical effects at a caustic by showing that the contribution to the propagator per degree of freedom should go as $\hbar^{1/2}$ rather than $\hbar^{1/3}$ [3] within a "critical region" [4] of the caustic where the actions of the direct and reflected paths differ by less than $\hbar$.

Despite the dynamical sense conveyed by the term "mixing," most studies of the inhibition of mixing in quantum chaos have explored either the statistics of energy levels or the spatial localization of eigenstates for (bounded) conservative systems. Localization, or "scarring," of chaotic eigenstates was first observed by Heller for the stadium billiard [5], a strongly chaotic system with isolated unstable periodic orbits. Heller's scars are local enhancements above the background intensity that occur along those orbits that are the least unstable—meaning that the ratio of the frequency of the orbit to the Lyapunov exponent that characterizes the divergence of adjacent trajectories is significantly greater than one [6]. A second mechanism for eigenstate localization has been observed by Bohigas *et al.* [7] in the soft chaos of two weakly coupled quartic oscillators. The local enhancements found in the eigenstates for this system arise from the quantization of the remnants of Kol'mogorov-Arnol'd-Moser (KAM) tori, or "cantori."

In contrast, we focus on the time domain rather than the energy domain, using semiclassical ideas to relate the quantum dynamics to the evolution of the classical Lagrangian manifold for a chaotic Hamiltonian system. In a recent publication [8] we discussed the role of classical phase space structures in the quantum evolution of a wave packet prior to the onset of chaos. In particular, we considered the motion of a quantum particle in a cosine potential perturbed by an external force varying sinusoidally in time. We posed the problem in the naive semiclassical limit where the natural length, mass, and time scales make $\hbar$ small. We studied the dynamics of a wave packet that was initially well localized in position and momentum and compared it to that of the classical distribution in phase space. Provided the classical distribution remains inside the separatrix of the unperturbed motion and avoids the hyperbolic fixed points on the separatrix, the two initially identical distributions were found to remain indistinguishable, even though both spread out to fill much of the initial well. However, when the Lagrangian manifold interacts with a hyperbolic fixed

point and acquires a tendril-like feature, the wave function was found to exhibit a persistent nodal structure that represents the first appreciable quantum effect with no classical analog. We also showed that this feature is relatively benign, having little impact on the physical observables.

In this paper we consider essentially the same system but focus our attention on the classical exit event when a substantial fraction of the classical distribution crosses the separatrix and leaves the well, marking the onset of chaos. Here we will show that the apparent equivalence of the quantum and classical distributions rapidly disintegrates when a "turning point" in the Lagrangian manifold that corresponds to a true caustic moves past a hyperbolic fixed point and outside the initial well. Specifically, we observe that while the peak in the classical probability density associated with the caustic follows the caustic out of the well, the peak in the quantum distribution becomes pinned at the top of the barrier. This pinning effect represents a specific dynamical mechanism for the quantum inhibition of classical mixing in a time-dependent Hamiltonian system.

We have deliberately chosen to study a time-dependent Hamiltonian with one degree of freedom because it is sufficiently complex to exhibit chaos yet simple enough to be studied directly in phase space. We point out that this problem is not equivalent to the conservative two-dimensional problem obtained by elevating time to the role of an additional degree of freedom because of the distinct role of time as a parameter rather than an operator in quantum mechanics. The quasiconservative system that one obtains by invoking the strobed-time Floquet formalism [9] is not relevant to our problem either since the phenomena we observe occur on a time scale that is a fraction of the period of the driving and cannot be discussed meaningfully in terms of the quasienergy Floquet states. Not being constrained by the symmetry of a time-invariant Hamiltonian, the mechanisms we observe are not limited to conservative systems and may in fact be disallowed by that symmetry in certain cases.

Although the origin of the pinning effect, like the nodes of our previous paper, can be understood semiclassically, the origins of the two effects are distinctly different. The nodes in Ref. [8] were shown to be the result of a beating phenomenon in the Van Vleck–Gutzwiller (VVG) propagator [10] between paths having the same Gutzwiller phase. The most prominent nodes were found to be the closest in action to a false caustic in the flow field which developed as a result of the interaction of the Lagrangian manifold with the hyperbolic fixed point. In contrast, the structure we observe here is a result of interference between direct and reflected paths—which differ by $\pi/2$ in Gutzwiller phase—and the most prominent structure is in the neighborhood of a true caustic.

Because the stationary paths in the path integral converge at a caustic, the stationary phase approximation that leads to the VVG propagator by summing each classical path independently breaks down. Therefore, to discuss the behavior near the caustic, we adopt a semiclassical propagator derived by Schulman [3] that is strictly valid only in the immediate vicinity of a caustic. Since this propagator cannot be evaluated numerically as easily as the VVG propagator, we develop an approximate "connection formula"— similar in spirit to the WKB connection formulas—to evaluate the Schulman propagator from the VVG expression. This yields an expression that is valid even at the caustic. We use this hybrid propagator to show that the differences between the classical and quantum behavior associated with the classical exit event can be understood semiclassically in terms of the area-preserving deformation of the manifold.

Furthermore, our propagator can be used to study the exponential tail of the wave function in the shadow or classically forbidden region of the caustic which is missed completely by the VVG propagator. This is important to our problem since the stretching of the exponential tail is the primary semiclassical mechanism for the quantum system to explore the world outside the remnant separatrix. Hence the VVG propagator, which puts zero amplitude in the classically forbidden region, becomes inadequate to describe the dynamics of the wave packet after the exit event. We point out that this failure of the VVG propagator is not necessarily inconsistent with the long-time accuracy achieved by Tomsovic and Heller [11] in the case of the stadium billiard. Since the amplitude in the forbidden regions is evidently negligible in that problem [4], it follows that the stretching of the exponential tail and associated phenomena that we observe must not be significant there.

The main body of this paper is organized as follows. In Sec. II we describe the Hamiltonian, the choice of initial conditions, and the method of analysis. (The present discussion is rather brief, since a complete discussion is contained in Secs. II and III of Ref. [8].) We explain our semiclassical analysis in Sec. III and in Sec. IV we present our results. We close in Sec. V with a summary of our results and some concluding remarks.

II. PROBLEM

We study the motion of a particle of mass 1/2 in a cosine potential subject to a sinusoidally driven external force. The Hamiltonian is given by

$$H(p,x,t) = p^2 - \frac{1}{2}\cos(\pi x) - \epsilon x \sin(\omega t + \phi) \qquad (1)$$

with $\omega = 2.5$, $\epsilon = 0.126$, and $\phi = 1.5493$. We include the nonzero constant ϕ [12] to make contact with the calculation of Ref. [8]. For these choices of ω and ϵ [13] the external force may be considered as a small perturbation in the context of KAM theory [14], and we are justified in discussing the dynamics in the context of the remnant orbit structure of the unperturbed motion. The separatrix at the threshold energy of the cosine potential plays a particularly important role in the onset of the chaos, being the first orbit to rupture but the last to fully disintegrate as a result of the perturbation. This orbit is shown in Fig. 1(a) with the hyperbolic (unstable) fixed points and the stable and unstable manifolds labeled accordingly.

In this paper we study the dynamics for initial con-

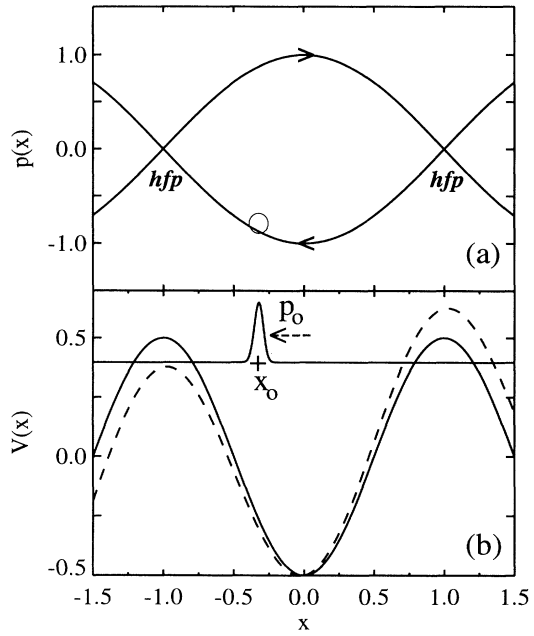

FIG. 1. (a) Unperturbed separatrix at zero energy showing the stable and unstable manifolds of the hyperbolic fixed points at $x = \pm 1$. The location and size of the initial wave packet are given by the three sigma ellipse centered at $(p_0, x_0) = (-0.7889, -0.3215)$ for comparison to the dot plot representation in Fig. 3(a). (b) The unperturbed (solid) and perturbed (dashed) potentials $V_0(x) = \frac{1}{2}\cos(\pi x)$ and $V(x,0) = V_0(x) - \epsilon x \sin(\phi)$ with a schematic depiction of the initial wave packet.

ditions in the neighborhood of the point $(p_0, x_0) = (-0.7889, -0.3215)$. The trajectories starting in this neighborhood, being very near the separatrix, rapidly lead to unbounded motion at $t_{ex} \approx 2.5$. (Note that the exit time $t_{ex} \sim T$, where $T = 2\pi/\omega$ is the period of the external force.) This choice of initial conditions allows us to examine the escape event associated with the onset of chaos with a minimum of computational effort.

To study the quantum evolution, we propagate an initial wave function forward in time by the split operator method [15] generalized to time-dependent systems. Our choice of $\hbar = (200\pi)^{-1}$ sets the quantum length scale for the problem to be small compared to the scale of variation in the potential. This allows us to pick an initial wave function that is initially well localized in both position and momentum. We choose for $\psi(x,0)$ a Gaussian wave packet of width σ centered at (p_0, x_0)

$$\psi(x,0) = (\pi\sigma^2)^{-1/4} \exp\left[-\frac{(x-x_0)^2}{2\sigma^2} + i\frac{p_0}{\hbar}(x-x_0)\right]. \tag{2}$$

The initial width $\sigma = 0.0225$ of the wave packet is chosen to be equal to that of the ground state wave function at the bottom of the cosine potential. We include one cosine well on each side of the well at the origin (three wells total) to avoid spurious interference between the escaping quantum amplitude and that remaining in the initial well due to the periodic boundary conditions imposed by the fast Fourier transform algorithm. A schematic depiction of the initial wave function in the cosine potential is shown in Fig. 1(b). The solid curve gives the cosine potential $V_0(x)$, while the dashed curve gives the complete time-dependent potential $V(x,0) = V_0(x) - \epsilon x \sin(\phi)$. Accompanying the seesaw motion of the external washboard potential, the x coordinate of each hyperbolic fixed point at (p_h, x_h) oscillates sinusoidally in time with $x_h \approx \pm n - (2\epsilon/\pi^2)\sin(\omega t + \phi)$ $(n = 1, 3, 5, ...)$ and $p_h = 0$. The wave packet is launched in the negative x direction, as shown. After reflecting off the barrier at $x \approx -1$ (which rises in time to meet it), it subsequently scatters off the top of the barrier at $x \approx +1$, where it is partially transmitted.

To study the classical evolution, we evolve the classical equations of motion forward in time for a set of 10 000 "particles" with different initial conditions. To ensure that the classical and quantum descriptions agree initially, the initial conditions are drawn at random from a two-dimensional Gaussian distribution of initial conditions centered at (p_0, x_0) and having widths in p and x equal to the widths in momentum and position of the initial wave function of Eq. (2). We compare the classical evolution to the time-evolved quantum probability density $P_{qm}(x,t) = |\psi(x,t)|^2$ by making a histogram with respect to x of the time-evolved classical distribution.

III. SEMICLASSICAL ANALYSIS

We remind the reader that the time-evolved wave function is found from the initial wave function $\psi(x,0)$ and the propagator as follows:

$$\psi(x,t) = \int dx'\, G(x,x';t)\, \psi(x',0). \tag{3}$$

For our semiclassical analysis, we require an accurate approximation to the propagator. Far from a caustic, we use the well-known propagator due to Van Vleck and Gutzwiller [10]

$$G_{\mathrm{VVG}}(x,x',t) = \sum_{\text{cl paths}} \left(\frac{1}{2\pi i\hbar}\right)^{1/2} \left|\frac{\partial^2 S(x,x',t)}{\partial x \partial x'}\right|^{1/2} \times \exp\left(i\frac{S(x,x',t)}{\hbar} - i\nu_t\frac{\pi}{2}\right), \tag{4}$$

while close to a caustic we employ an expression for the propagator due to Schulman [3]

$$G_{\mathrm{Sch}}(x,x',t) = \left(\frac{1}{2\pi i\hbar}\right)^{1/2} \left|\frac{\lambda(x,x',t)}{(\partial^2 S/\partial x \partial x')^{-1}}\right|^{1/2}_{x=x_c} \times \mathrm{Ai}(z) \exp\left(i\frac{S_c + p_c(x-x_c)}{\hbar}\right). \tag{5}$$

In these two expressions $S(x,x',t)$ is the classical action as a function of the initial (x') and final (x) positions,

$S_c = S(x_c, x', t)$ and (p_c, x_c) respectively give the action and phase space coordinates at the caustic, and ν counts the number of times the trajectory connecting x' and x encounters a caustic where $\nu\pi/2$ is the "Gutzwiller phase." The argument $z(x, x', t)$ of the Airy function in Eq. (5) is found [16] by solving the boundary value problem for the quantum fluctuations around the classical trajectory $x(x', t)$ [3] to obtain the eigenvector with the lowest eigenvalue $\lambda_1 \propto \lambda(x, x', t)/t^2$. While both the numerator and denominator in the prefactor of Eq. (5) separately vanish at $x = x_c$, their ratio is finite so that the singularity in Eq. (4) at $x = x_c$ is absent.

Both of these expressions represent a WKB approximation to the exact propagator [3], meaning that the path integral is evaluated by the method of steepest descents [17]. The former, which assumes that the stationary paths are well separated, is valid when the relative action for any two paths is much greater than $\hbar$, while the latter, which assumes that two of the stationary paths are coalescing at a caustic, is valid only in the immediate vicinity of the caustic.

As an initial value problem, implementing the propagator of Eq. (4) is a very reasonable task in one dimension for short times, even when the dynamics are chaotic, and one can often get away with simply ignoring the caustic spikes associated with the singularity in the prefactor [11]. Unfortunately, as we mentioned above in Sec. I, we do not find this to be the case for our problem. But an exact calculation of Eq. (5) is basically untenable because of the need to solve a boundary value problem at each point in space. To avoid this, we approximate $G_{\rm Sch}$ by relating it asymptotically to $G_{\rm VVG}$. The validity of this approximation rests on being able to find a region not too close to the caustic where both $G_{\rm VVG}$ and $G_{\rm Sch}$ are reasonably accurate in order to match them, similar in spirit to the usual WKB connection formulas for semiclassical wave functions [2]. This "connection formula" gives the argument of the Airy function in terms of the action difference between the direct and reflected paths. Thus one has only to solve the classical equations of motion (an initial value problem) and compute the action along the classical paths to evaluate $G_{\rm Sch}$.

For our problem, the initial wave function of Eq. (2) is sufficiently localized at $x' = x_0$ that near the caustic we may approximate $\psi(x, t)$ in Eq. (3) by $G(x, x_0, t)$ directly. In Eq. (5) we take z to be sufficiently large and negative (more precisely $|z|^{-3/2} \ll 1$) to replace $\mathrm{Ai}(z)$ with its leading asymptotic expansion. Also, we assume that the sum over classical paths in Eq. (4) consists of a single pair of direct and reflected paths and that the prefactors for these two paths are equal.

In this approximation we find that

$$|G_{\rm VVG}(x,t)|^2 = \frac{1}{2\pi\hbar}\left|\frac{\partial^2 S(x,x',t)}{\partial x \partial x'}\right|_{x'=x_0} \times\left[1+\cos\left(\frac{\Delta S(x)}{\hbar}-\frac{\pi}{2}\right)\right] \qquad (6)$$

and

$$|G_{\rm Sch}(x,t)|^2 \propto |z(x)|^{-1/2}\left[1+\cos\left(\frac{4}{3}|z(x)|^{3/2}-\frac{\pi}{2}\right)\right], \qquad (7)$$

where $\Delta S(x) = S_r(x, x_0, t) - S_d(x, x_0, t) \geq 0$. (The subscripts d and r denote the direct and reflected paths, respectively.) By comparing the cosine arguments for Eqs. (6) and (7) one obtains the relation $z(x) = -[3\Delta S(x)/4\hbar]^{2/3}$. Although the condition $|z|^{3/2} \ll 1$ is satisfied (to about 1%) only if $\Delta S/\hbar > 2\pi$, we find that using this expression for z in Eq. (5) works remarkably well even as $\Delta S/\hbar \Rightarrow 0$. For the shadow region of the caustic ($x > x_c$) we estimate the magnitude of $z = +|z|$ by reflecting the action difference about the caustic, i.e., we take $\Delta S(x) = \Delta S(x - x_c)$. We cannot infer the constant prefactor of Eq. (5) in a similar manner because the quantity $|z|^{-1/2} \approx (3\Delta/4\hbar)^{-1/3}$ only crudely mimics the behavior of the VVG prefactor as $x \Rightarrow x_c$.

To evaluate $|G_{\rm VVG}|^2$ and $|G_{\rm Sch}|^2$ according to Eqs. (6) and (7) we evolve the vertical strip of phase space defined by $x' = x_0$ forward in time according to the classical equations of motion. At the desired time we obtain the action $S(x, x', t)$ and its mixed partial derivative $\partial^2 S(x, x', t)/\partial x \partial x' = -\partial p'(x, x', t)/\partial x$ as functions of x for the direct and reflected paths by interpolating between the time-evolved grid points representing the strip. Given these quantities, the rest of the calculation is straightforward.

Although we have argued that the VVG propagator fails near caustics, the overall character of the wave function is often preserved despite the presence of caustic spikes. Even when the wave function is piled up at the caustic, so that the effect cannot be ignored, the problem is often temporary, disappearing once the amplitude has scattered away. However, when there is a sustained accumulation of amplitude at the caustic like we see in our problem, the VVG propagator becomes inadequate.

To demonstrate this worst case scenario, we compare $|\psi(x,t)|^2$ for the full quantum calculation to both the VVG and Schulman expressions for $|G(x, x_0, t)|^2$ at $t = 3$, as shown in Fig. 2. Both curves are matched onto the full

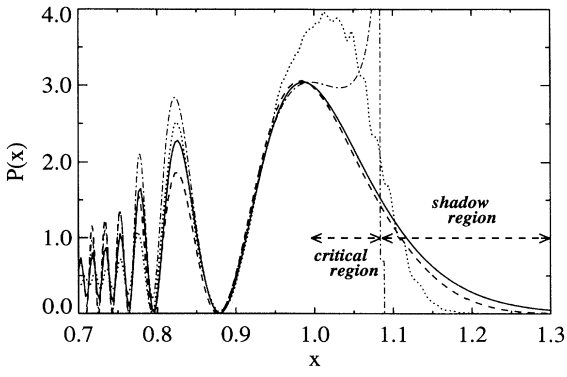

FIG. 2. Comparison of $P_{qm}(x,t)$ (solid curve) to $|G(x,x_0,t)|^2_{\rm VVG}$ (dash-dotted curve) and $|G(x,x_0,t)|^2_{\rm Sch}$ (dashed curve) at $t = 3$. Also shown is the cellular dynamics calculation of the VVG probability density (dotted curve).

quantum calculation at the primary maximum ($x \approx 0.89$) to determine the "correct" prefactors [18]. This is necessary because we do not know the Schulman prefactor and, being so close to a caustic, we cannot trust the VVG prefactor. For the sake of comparison we also integrate Eq. (3) numerically for the VVG propagator using Heller's cellular dynamics method [19]. (We cannot do the same for the Schulman propagator because our method of approximation suppresses both the phase information and the prefactor which depend on p_0.) The critical and shadow regions of the caustic at $x_c \approx 1.09$ are indicated on the the plot.

Comparing the VVG and Schulman expressions for $|G(x, x_0, t)|^2$ to the true quantum probability density, we see that the VVG expression gets the oscillations to the left of the caustic about right, but it fares badly in the critical region of the caustic, as expected, and it lacks an exponential tail altogether. The Schulman expression, on the other hand, not only gets the oscillations about right, but also correctly describes the exponential behavior at the caustic and into the shadow region where $z(x) > 0$. In the cellular dynamics calculation the spurious singularity in the integrand causes the primary peak to have too much amplitude and to be shifted to the right, and the change in the location of the caustic across the set of time-evolved vertical strips that contribute to the integral gives rise to a tail in the shadow region that poorly approximates the true feature. While the integration smears the singularity out, it clearly does not fix the problem.

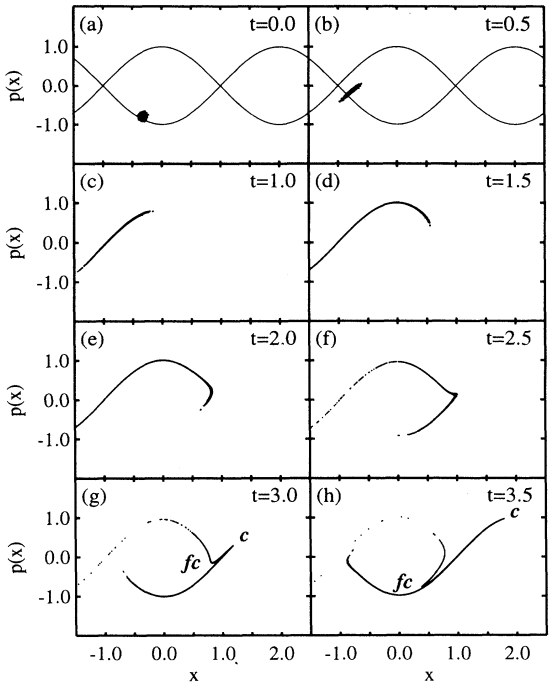

FIG. 3. (a)–(h) Time evolution of the Gaussian phase space distribution at increments of $\Delta t = 0.5$. The "tendril" as discussed in the text refers to the feature in the distribution between the caustic (at c) and the false caustic (at fc) in (g) and (h).

IV. RESULTS

In order to discuss the quantum dynamics of this system in a semiclassical context, it is necessary that we first point out several features of the classical flow as it approaches and interacts with the hyperbolic fixed points. In Figs. 3(a)–3(h) we show the time evolution of the classical phase space distribution for $t = 0.0$–3.5 at intervals of $\Delta t = 0.5$ (≈ 0.2 T). Each dot represents the time-evolved coordinates for one of the 10 000 particles in the distribution. We superimpose the separatrix of the unperturbed problem in the first two frames for reference, and in the last two frames we indicate both the caustic (at c) and the feature that we call the false caustic (at fc).

First, the initially compact object rapidly spreads out along the remnant separatrix, being stretched by the unstable manifold of the hyperbolic fixed point at $x \approx -1$, as shown in Figs. 3(a)–3(d). As a result, the particles appear to be following the same (threshold) orbit in Fig. 3(e). They in fact approach the hyperbolic fixed point at $x \approx +1$ with a fraction of the original energy dispersion. This behavior is distinctly different from the spreading that occurs in the absence of the time-dependent perturbation and is not just a consequence of the orbital period being time dependent.

Second, the bright side of the caustic ($x < x_c$) is not restricted to the inside of the initial well ($x < x_h \approx 1$), as shown in Figs. 3(g) and 3(h). The phase space coordinates of the caustic have clearly crossed the separatrix in both cases. The remnant separatrix is thus only a "partial barrier to transport" [20] that temporarily confines the phase space flow, and the interaction of the flow with the hyperbolic fixed point is the door to the region of phase space that was inaccessible in the absence of chaos. Here we note that the classical dynamics does not achieve local mixing inside the remnant separatrix prior to the exit event, in contrast to the analysis of Bohigas *et al.* [21] which assumes that local mixing is well established before regions separated by partial transport barriers communicate with each other.

Third, the tendril that results from the interaction of the flow with the hyperbolic fixed point—meaning the feature in the Lagrangian manifold between the caustic and the false caustic in Figs. 3(g) and 3(h)—gets thinner and longer as a function of time. The tendril is thus acting like a closed curve in phase space whose enclosed area is conserved by Liouville's theorem. Neglecting the term $\int \Delta H(t) dt \propto \epsilon$ that follows from the inexact cancellation of the time-dependent potential along the two paths [8], the area "enclosed" by the tendril $\Delta A = \int_{x_c}^{x_{fc}} \Delta p(x) dx$ is indeed approximately given by the relative action between the two paths at the false caustic $\Delta S(x_{fc}, x')$, where (p_{fc}, x_{fc}) denote the coordinates of the false caustic.

The false caustic is a fold or "turning point" in the Lagrangian manifold that does not correspond to a real caustic, meaning that the caustic count ν is not incremented by one there, but rather is decremented by one.

[In Fig. 3(g) the fold is actually just on the verge of forming.] Particles do not flow around this fold as a function of time. Rather, those in the immediate vicinity of the false caustic move rigidly with the manifold as it deforms. Consequently, the quantity $\Delta S(x_{fc}, x')$ approaches a constant value as the gap between the two paths at the false caustic closes. Since $\Delta S(x_{fc}, x') \approx \Delta A$, we see that the area-preserving nature of the flow that gives rise to the stretching of the tendril is closely tied to the existence of the false caustic in the Lagrangian manifold.

Having discussed some general features of the classical flow, we now examine the corresponding quantum and classical probability densities shown in Figs. 4(a)–4(h). We see that the classical and quantum distributions are essentially indistinguishable for $t < 2$, but that this equivalence disappears once the tendril forms and the classical motion becomes unbounded ($t > 2$). We should also point out that, while some of the particles appear to escape the well to the left at $t \approx 1$, they subsequently get pulled back inside [see Figs. 3(c)–3(e) and 4(c)–4(e)]. This spurious escape event, unlike the real event, is not accompanied by any folding of the Lagrangian manifold and the equivalence of the quantum and classical distributions is preserved.

Just prior to the departure of the quantum from the classical behavior at $t \sim 2.5$ we see that x_c and x_h are nearly coincident, as are the quantum and classical maxima. The caustic then moves off in the positive x direction away from the hyperbolic fixed point and the classical maximum follows. The quantum maximum, however, is left behind, stuck on top of the cosine barrier. This pinning of the quantum peak on the barrier, as a mechanism for the inhibition of mixing, is the key feature that we observe in the quantum chaotic dynamics of this system.

We emphasize that this sticking or pinning phenomenon is not a result of the difference in quantum and classical transmission coefficients for a cosine barrier—which is negligible for our value of $\hbar$. In particular, we find no appreciable difference between time-evolved quantum and classical probability densities when we scatter a Gaussian wave packet off an isolated, rigid cosine barrier at the threshold energy. Nor is the pinning caused by the side-to-side and/or up-and-down motion of an isolated potential barrier. If we mimic the oscillations in position and energy near the hyperbolic fixed point of the perturbed cosine potential with a potential barrier of the form $[1 + S(t)]\cos[kx - R(t)]$, we again find no appreciable difference between the quantum and classical scattering at near-threshold energies. We conclude that the history of the wave packet in the cosine well, particularly its delocalization prior to the escape event, is crucial in giving rise to the differences between the classical and quantum distributions that we observe.

Ironically, the delocalization of the wave packet is, in the following sense, related to eigenfunction localization. Having noted that the classical phase space distribution of Fig. 3(a) evolves to resemble the separatrix, one might expect the corresponding time-evolved wave functions to resemble the near-threshold eigenstates of the unperturbed Hamiltonian. Quite generally, for potentials with local maxima (or saddle points in two or more dimensions) at energies well above the ground state energy, the near-threshold eigenstates are highly peaked or "localized" at the potential energy maxima [22]. This feature is clearly manifested in the wave functions of Figs. 4(e)–4(h). The overlap of the still localized wave packet and the extended threshold eigenfunction is small in Figs. 4(a) and 4(b), but as the wave packet spreads out along the separatrix, the overlap increases. Thus the accumulation of amplitude at the hyperbolic fixed point represents the propensity for the chaotic dynamics to increase the overlap between the evolving wave function and the threshold eigenstates. In this sense, the stickiness of the hyperbolic fixed point that gives rise to the pinning effect is a time-dependent manifestation of eigenfunction localization.

We emphasize that the pinning effect occurs on a time scale short compared to the period of the driving. If one were to study the strobed dynamics of our time periodic Hamiltonian at long times, one would expect the Floquet states rather than the eigenstates of the unperturbed problem to govern the (coarse-grained) dynamics, particularly the Floquet states having the greatest overlap with the initial state. An analysis of the strobed-time quantum map, like those of Geisel *et al.* [23] and Spina and Skodje [24] for the quantum kicked rotor, would miss this effect entirely.

The pinning effect can also be understood dynamically

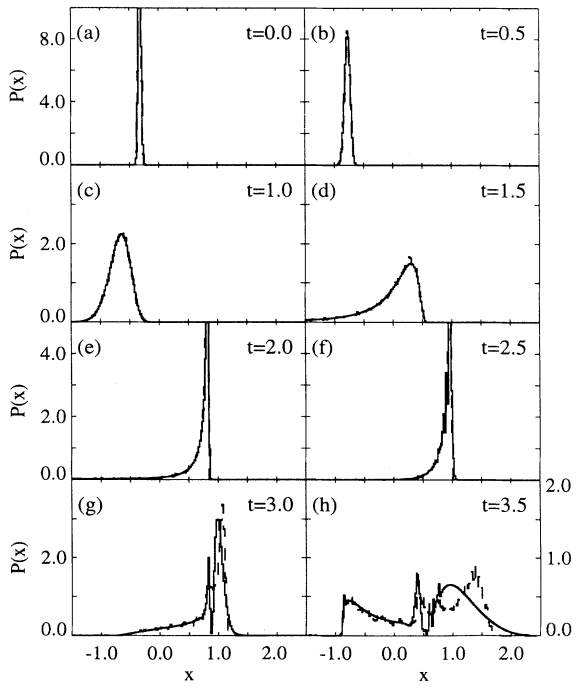

FIG. 4. (a)–(h) Time evolution of $P_{\rm cl}(x,t)$ (dashed curve) and $P_{qm}(x,t)$ (solid curve) at increments of $\Delta t = 0.5 \approx 0.2$ T. Note the divergence of the classical and quantum maxima that occurs in (g) and (h) accompanying the emergence of the tendril in Fig. 3.

as a quantum interference effect between paths in the semiclassical propagator. The interference we see does not result from a wave packet that splits while interacting with a hyperbolic fixed point and later recombines at another hyperbolic fixed point [24]; rather, the interference occurs at the first interaction with a hyperbolic fixed point and between very similar paths. To explain this we focus on the tendril feature in the region of the caustic just after the escape event (at $t = 3$). We show the quantum and classical probability densities as well as the Schulman WKB approximation of Eq. (7) in Fig. 5(a) and the corresponding classical phase space distribution in Fig. 5(b). In Fig. 5(c) we plot the relative action $\Delta S(x)$ and VVG path amplitude $|\partial^2 S/\partial x \partial x'|^{-1/2}_{x'=x_0}$ for the time-evolved vertical strip $p(x, x_0)$. The direct and reflected paths and the locations of the caustic (c), false caustic (fc), and x coordinate of the hyperbolic fixed point are indicated accordingly.

The agreement between the quantum distribution and the WKB approximation in Fig. 5(a) clearly demonstrates that the structure of the wave function in the vicinity of the tendril has a semiclassical origin. Specifically, the oscillatory nature of the wave function here is caused by interference between the two nearby paths that comprise the tendril. These paths do not contribute to the propagator independently, however, because of the proximity of their actions [see Fig. 5(c)], which is why we must use Schulman's approximation to the two-path WKB propagator to describe the interference properly. Our semiclassical analysis is only valid in the region $x > x_{fc}$, however, because of the sudden divergence of the VVG amplitudes to the left of the false caustic [see also Fig. 5(c)]. We observe similar agreement between the quantum distribution and Schulman's approximation at $t = 2.5$ and $t = 3.5$, although the presence of additional paths complicates matters somewhat in the latter case.

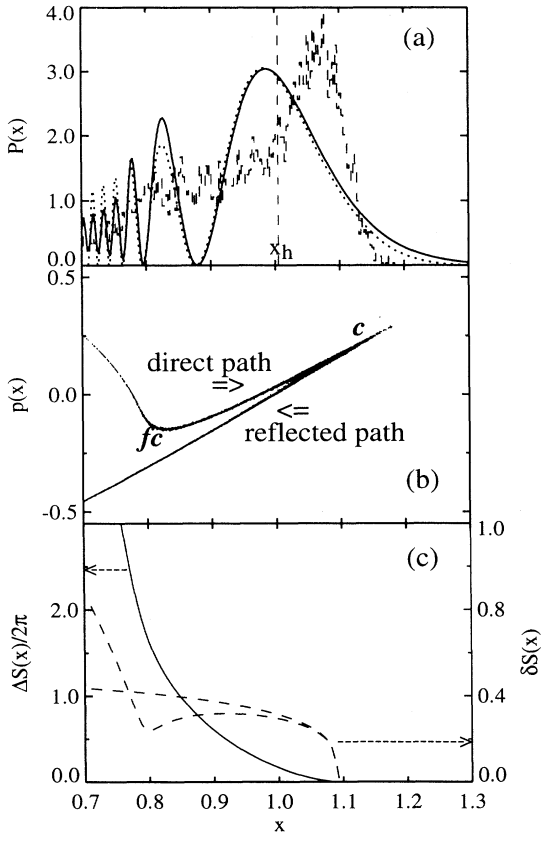

FIG. 5. (a) Same curves of Fig. 4(g) magnified to show the structure associated with the tendril. Also shown is the semiclassical approximation $|\psi|^2 \sim |G_{\rm Sch}|^2$ as described in Sec. III (dotted curve). (b) The corresponding phase space distribution of Fig. 3(g). (c) The relative action $\Delta S(x)/2\pi$ in units of $\hbar$ (solid curve) and the (inverse) VVG amplitude $\delta S(x) \equiv \sqrt{2\pi\hbar}\,|\partial^2 S/\partial x \partial x'|^{-1/2}_{x'=x_0}$ along the direct and reflected paths (dashed curves).

The region for which $\Delta S(x, x')/\hbar < 1$—or equivalently, the region where Schulman's propagator should replace the VVG propagator—grows directly with the length of the tendril. Since the area enclosed by the tendril ΔA is roughly constant in time with $\Delta A \approx \Delta S(x_{fc}, x')$, as explained above, it follows that the Airy structure associated with the tendril simply gets stretched as the tendril is stretched. As a result, the quantum peak remains near $x_h \approx +1$ where it originated. The area-preserving nature of the chaotic Hamiltonian flow, coupled with the presence of the false caustic in the Lagrangian manifold, is thus responsible for the peak in the quantum distribution being held at the hyperbolic fixed point, thereby inhibiting the quantum transport of probability across the separatrix.

V. CONCLUSIONS

We have shown that the quantum probability density rapidly diverges from that of the analogous classical system when the tendril formed by the interaction of the Lagrangian manifold with the hyperbolic fixed point leads to (classically) unbounded motion. We have also shown that this divergence is the consequence of a quantum interference effect that pins the quantum peak associated with the caustic at the top of the potential barrier. This pinning effect is a concrete example of how quantum interference suppresses the exploration of "phase space" outside the broken separatrix to inhibit the classical mixing.

The origin of the pinning effect was shown to be semiclassical, resulting from interference in the propagator between the direct and reflected paths associated with the tendril. We found it necessary to use an approximation to the WKB propagator due to Schulman that is valid near caustics, rather than the Van Vleck-Gutzwiller propagator, in order to study this interference properly. This is because the stretching of the tendril that accompanies the chaotic dynamics phase locks the entire region of phase space explored by the tendril in close proximity to the caustic. We approximate Schulman's propagator by relating its asymptotic expansion to the Van Vleck–Gutzwiller propagator. This avoids the untenable boundary value problem one must otherwise solve in order to calculate Schulman's propagator directly. We have

shown that Schulman's propagator, evaluated in this way, accounts for the difference between the behavior of the quantum and classical systems at the times we consider.

We emphasize that this interference occurs between direct and reflected paths, differing in Gutzwiller phase by $\pi/2$—in contrast with the interference effect discussed in Ref. [8]. Thus we conclude that the interference between direct and reflected paths (for these very early times) has no permanent effect on the wave function as it sloshes back and forth in the potential well as long as the classical motion remains bounded—just as the structure that appears in a wave packet as it scatters off of a rigid barrier [2] is temporary, disappearing once the packet is fully reflected. When the motion becomes unbounded, however, we have shown that the interference between direct and reflected paths in the tendril permanently modifies the wave function, profoundly affecting the quantum-classical equivalence that characterizes the dynamics prior to the exit time. We have shown that this divergence of the quantum and classical behavior is a direct consequence of the folding and stretching of the Lagrangian manifold that accompanies the classical flow across the separatrix and this, in turn, is a direct consequence of the onset of the classical chaos.

Because the pinning effect is directly related, in the semiclassical sense, to generic features of the classical Hamiltonian chaos, we argue that this mechanism for the inhibition of mixing is itself generic. Thus one should expect to find the pinning effect in other weakly driven chaotic Hamiltonian systems as well. Moreover, since classical canonical perturbation theory and the KAM theory for the origin of soft chaos are applicable for both time-dependent and time-independent perturbations [25], this mechanism should also appear in conservative (Hamiltonian) systems characterized by soft chaos. Lacking the time dependence responsible for the false caustic in our problem, we suspect that the higher-order caustics (where the caustic count ν changes by more than one) that can exist in such systems because of the increased dimensionality would play the role of the false caustic in giving rise to the pinning effect.

We cannot go so far as to argue that the pinning effect is generic to all Hamiltonian quantum chaos, however, because the presence of tendrils and either false caustics or (possibly) higher-order caustics in the Lagrangian manifold is not, by itself, sufficient to produce this feature. The partial barrier to classical phase space transport associated with the broken separatrix appears to be the more crucial element. While the strongly chaotic stadium billiard problem, for example, exhibits both higher-order caustics [4] and tendril-like structures (see the two-dimensional Birkhoff projection of the Lagrangian manifold in Ref. [4]), it does not possess the simple KAM structures (i.e., the cantori or broken separatrices) that act as partial barriers to transport [20]. Nor does the quantum system manifest the stretching of the exponential tail in the classically forbidden region (or the associated pinning effect), or so we assume given the long-time accuracy of the VVG propagator achieved by Tomsovic and Heller for that problem mentioned in Sec. I. But whether or not this mechanism is significant in other systems characterized by hard chaos is still an open question.

ACKNOWLEDGMENTS

We would like to thank Steve Tomsovic and Harold Baranger for useful discussions. We would also like to thank Vijay Poduri for bringing our attention to Ref. [3]. This work was supported by the National Science Foundation under Grant No. DMR–9020310.

[1] M. V. Berry, N. L. Balazs, M. Tabor, and A. Voros, Ann. Phys. (N.Y.) **122**, 26 (1979).

[2] L. I. Schiff, *Quantum Mechanics* (McGraw-Hill, New York, 1968), Chap. 6.

[3] L. S. Schulman, in *Functional Integration and Its Applications*, edited by A. M. Arthurs (Oxford University Press, London, 1975), and references therein; *Techniques and Applications of Path Integration* (Wiley, New York, 1981), Chaps. 3 and 13–15.

[4] S. Tomsovic and E. J. Heller, Phys. Rev. E **47**, 282 (1993).

[5] E. J. Heller, Phys. Rev. Lett. **53**, 1515 (1984).

[6] E. J. Heller, in *Chaos and Quantum Physics*, edited by M. J. Giannoni, A. Voros, and J. Zinn-Justin, 1989 Les Houches Lectures Session LII (Elsevier, Amsterdam, 1991).

[7] O. Bohigas, S. Tomsovic, and D. Ullmo, Phys. Rep. **223**, 43 (1993).

[8] B. S. Helmkamp and D. A. Browne, Phys. Rev. E **49**, 1831 (1994).

[9] Y. B. Zel'dovich, Zh. Eksp. Teor. Fiz. **51**, 1492 (1966) [Sov. Phys. JETP **24**, 1006 (1967)].

[10] J. H. Van Vleck, Proc. Natl. Acad. Sci. U.S.A. **14**, 178 (1928); M. C. Gutzwiller, J. Math. Phys. **8**, 1979 (1967).

[11] S. Tomsovic and E. J. Heller, Phys. Rev. Lett. **67**, 664 (1991).

[12] In order to amplify the interesting behavior associated with the classical exit event for the initial conditions of Ref. [8], we followed the unstable classical trajectory used in Ref. [8] up to a time $t = 12/\pi$ shortly before the classical exit event and launched a localized wave packet there.

[13] W. A. Lin and L. E. Reichl, Phys. Rev. A **37**, 3972 (1988).

[14] M. C. Gutzwiller, *Chaos in Classical and Quantum Mechanics* (Springer, Berlin, 1990).

[15] M. D. Feit, J. A. Fleck, Jr., and A. Steiger, J. Comput. Phys. **47**, 412 (1982).

[16] In Schulman's notation the prefactor in Eq. (5) is given (up to an overall time-dependent "constant") by $\sqrt{\lambda_1/f(t)}$. λ_1 is found by solving the equation for the Jacobi field ϕ $m\ddot{\phi} + \partial^2 V/\partial x^2|_{x_{\rm cl}}\phi + \lambda_n\phi = 0$ with $\phi(0) = \phi(t) = 0$ and $\lambda_1 < \lambda_2 < \cdots$, while $f(t)$ is found from the initial value problem $m\ddot{f} + \partial^2 V/\partial x^2|_{x_{\rm cl}} f = 0$ with $f(0) = 0$ and $\dot{f}(0) = 1$. Our form for the propagator in Eq. (5) follows given that $f(t) \equiv -m(\partial^2 S/\partial x \partial x')^{-1}$. (See Ref. [3], Chaps. 12, 13, and 15.)

[17] C. Chester, B. Friedman, and F. Ursell, Cambridge Philos. **53**, 599 (1957).

[18] It is not possible to match these curves to each other directly by insisting the wave function be normalized because the WKB propagator—which includes the VVG and Schulman expressions as limiting cases—is not in general unitary. Unitarity is only preserved when the WKB propagator happens to be exact—as for quadratic potentials.

[19] E. J. Heller, J. Chem. Phys. **94**, 2723 (1991). In our calculation we take $\alpha = \beta = 32/\sigma^2$, where α and β are the adjustable cell parameters discussed in the reference and σ is the width of the wave packet in Eq. (2). See Ref. [8] for more detail.

[20] R. S. MacKay, J. D. Meiss, and I. C. Percival, Physica D **13**, 55 (1984); D. Bensimon and L. P. Kadanoff, *ibid.* **13**, 82 (1984); R. S. MacKay, J. D. Meiss, and I. C. Percival, *ibid.* **27**, 1 (1987).

[21] See p. 124 of Ref. [7].

[22] A. R. P. Rau, Rev. Mod. Phys. **64**, 623 (1992).

[23] T. Geisel, G. Radons, and J. Rubner, Phys. Rev. Lett. **57**, 2883 (1986).

[24] A. Spina and R. T. Skodje, Comput. Phys. Commun. **63**, 279 (1991).

[25] B. V. Chirikov, Phys. Rep. **52**, 263 (1979).